Wavelet Transform and Machine Learning-Driven Multi-Class Classification of Chest X-Ray Images for COVID-19 Diagnosis

Amitesh Badkul

Ph.D. Programs in Computer Science
Department of Electrical and Electronics Engineering
BITS Pilani, Hyderabad Campus, India
f20180764@hyderabad.bits-pilani.ac.in

Vamsi Inturi

Mechanical Engineering Department
Chaitanya Bharathi Institute of Technology (A), Hyderabad, India
vamsismilebox@gmail.com

Radhika Sudha

Department of Electrical and Electronics Engineering
BITS Pilani, Hyderabad Campus, India
sradhika@hyderabad.bits-pilani.ac.in

Abstract

Chest radiography is a fast, low cost, and widely available first line test for suspected pneumonia and other respiratory infections, which makes automation clinically valuable where CT and subspecialty radiologists are limited. Yet adoption of automated CXR analysis using machine learning has been slowed by the memory and compute demands of large deep convolutional networks, their training time, and the need for GPU infrastructure, which limit deployment at the edge and in resource constrained settings. In acute care, separating COVID-19, bacterial pneumonia, and viral pneumonia is necessary for isolation, preventive care, so the classification is valuable and directly actionable by hospitals and clinics. We present a lightweight pipeline for multiclass CXR classification that applies a single level discrete wavelet transform and computes 11 statistical and texture descriptors per subband, producing a 44 dimensional feature vector for tabular classifiers. We evaluate CXRs stratified across four classes (healthy, COVID-19, bacterial pneumonia, viral pneumonia). Random Forest and XGBoost reach 96.83% and 97.76% test accuracy, respectively, outperforming transfer learned DCNN baselines on the same data. Ablations show that features pooled across subbands outperform any single subband and that texture descriptors including entropy, contrast, homogeneity, dissimilarity, and correlation carry most of the signal. Among wavelet bases, single level Bior6.8 performs best, while deeper decompositions reduce accuracy at this data scale. Because computation is limited to a grayscale wavelet transform and tabular learning, the method runs on commodity CPUs, has a small memory footprint, and is simple to reproduce, with strong per class performance for COVID-19, bacterial pneumonia, and viral pneumonia that supports further treatment.

1 Introduction

Machine learning is now deployed across medical diagnostics. It supports detection and risk prediction, and quick adaption has been accelerated with better datasets and algorithms. In medical imaging specifically, recent reviews describe a broad shift from pilot studies to clinically oriented evaluation and deployment [19]. Imaging has been a prime driver of this growth, especially in CT and chest radiography. CXRs are fast, inexpensive, and available at the point of care. Process improvements and digital mobile radiography have pushed turnaround for urgent CXRs from about an hour to well under half an hour in some settings, with minutes from obtaining to interpreting the final results [8].

Despite this progress, many CXR studies on COVID-19 frame the task as binary detection. Reviews note that binary designs are common, while multiclass separation remains less represented and more challenging [10]. In practice, hospitals need to distinguish COVID-19 from other pneumonias, especially bacterial and viral components for providing better care. A second limitation is reliance on large deep convolutional networks. Common backbones such as ResNet-50 have roughly 25 million parameters which translates into material memory and compute requirements. Even "mobile" families reduce but do not remove the need for specialized hardware during training, and can remain heavy at higher clinical resolutions. These demands slow iteration, raise costs, and complicate edge deployment in resource-constrained environments. Industry surveys also cite infrastructure and integration as adoption barriers.

To tackle the above limitations we introduce a lightweight pipeline that exceeds transfer-learned DCNN baselines. Our contributions include:

1. Lightweight CXR classification system. We introduce a compact pipeline based on a single level discrete wavelet transform and a small set of statistical and texture descriptors per subband, yielding a 44 dimensional feature vector for fast tabular learning on CPUs.

2. Better accuracy than DCNNs. On the same splits, Random Forest and XGBoost achieve 96.83% and 97.76% test accuracy, respectively, outperforming transfer-learned DCNN baselines.

3.

2 Literature Review

Panayides et al. [18] conducted a comprehensive review of state-of-the-art artificial intelligence (AI) solutions in medical imaging informatics, elucidating critical challenges in clinical translation and proposing forward-looking strategies to advance healthcare practice. The review underscores the imperative for robust medical data management frameworks and the seamless integration of AI into imaging workflows to enhance patient outcomes. Xu et al. [23] examined the transformative potential of generative AI within medical imaging, focusing on synthetic data generation, image enhancement, anomaly detection, and image-to-image translation. Their findings demonstrate that generative models, such as generative adversarial networks (GANs), substantially augment brain tumour datasets, fostering improved diagnostic accuracy and patient care. Mobarakeh et al. [14] provided an in-depth analysis of machine-learning methodologies for detecting, classifying, and segmenting COVID-19 in CT and X-ray imaging modalities. Their study highlights the efficacy of deep learning models in precisely delineating pathological lesions, empowering radiologists to make more accurate and efficient clinical decisions in diagnosing respiratory infections. Gadepally et al. [5] offered a case-based exploration of the generalizability of AI models in medical imaging, emphasizing the necessity of understanding algorithmic design, training data intricacies, and deployment environments. This review accentuates the importance of equipping radiologists with a nuanced understanding of the risks and benefits associated with AI algorithms to ensure their judicious and practical application in clinical settings. Li et al. [12] presented an exhaustive review of deep learning (DL) algorithms in medical image analysis, highlighting their profound impact on advancing diagnostic precision and operational efficiency. The study delineates the potential of cutting-edge DL methodologies to transform disease detection and optimize treatment planning paradigms. Kavitha and Inbarani [9] proposed an innovative hybrid framework that synergizes Bayes WT with convolutional neural networks (BayesWavT-CNN) to classify chest X-ray images into normal and COVID-19 categories. Their approach effectively attenuates image noise, culminating in
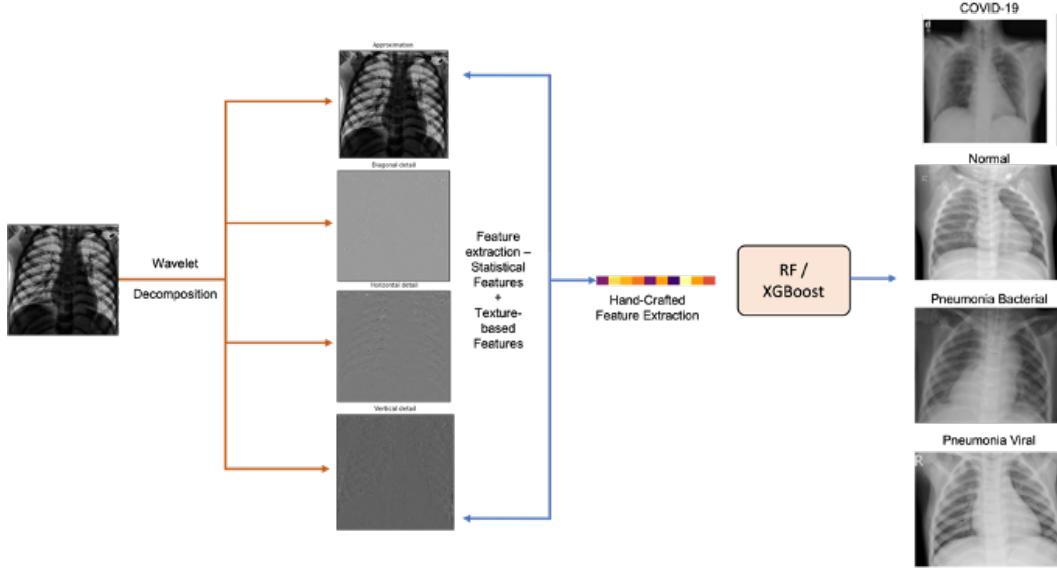
Figure 1: Framework followed in the current work: DWT-based decomposition to get sub-images (Approximation, Diagonal, Horizontal, and Vertical details), feature extraction (statistical and texture-based) and ML-based (RF and XGB) multi-class classification among COVID-19, Normal, Pneumonia Bacterial, and Pneumonia Viral.

enhanced classification accuracy. Abdel-Hamid [1] investigated the deployment of wavelet and contourlet trans-forms for COVID-19 classification in chest CT imaging. The study demonstrated that multiresolution analysis enables the segregation of diagnostically salient image fea-tures across distinct frequency subbands, thereby bolstering diagnostic accuracy. Yasar and Ceylan [24] developed an advanced deep-learning pipeline that integrates local binary pattern features, dual-tree complex wavelet transforms, and convolutional neural networks to detect COVID-19 in chest X-ray images. Their pipeline achieved high precision and demonstrated significant real-time applicability in identifying COVID-19 cases. Collectively, these investigations underscore substantial advancements in applying wavelet-based methodologies and deep learning architectures to medical image analysis, particularly in augmenting the detection and classification of COVID-19 through chest X-ray and CT imaging modalities.

3 Methods

3.1 Data and task

We study four-class chest-X-ray classification with labels Healthy, COVID-19, Bacterial pneumonia, and Viral pneumonia. The corpus contains 4,265 radiographs from [2]. We use a 70/30 stratified split with 2,986 images for training and 1,279 for testing. Images are treated as single-channel grayscale inputs.

3.2 Preprocessing

Each image is resampled to a fixed resolution, cast to 8-bit when needed, and normalized $[0, 1]$. We do not apply bone suppression or lung masking in the main pipeline. This keeps the system lightweight and isolates the contribution of multiresolution texture cues.

3.3 Discrete wavelet transform

We compute a single-level 2-D DWT that decomposes every CXR into four sub-bands: LL approximation, LH horizontal detail, HL vertical detail, and HH diagonal detail. The DWT implements a multiresolution, orientation-selective analysis that aligns with classical pyramid and quadrature-

filter theory and is widely used for texture and edge analysis [13]. Our primary mother wavelet is biorthogonal Bior6.8. Biorthogonal families admit symmetric, linear-phase analysis and synthesis filters that preserve edges and reduce phase distortion, properties that are desirable at lung borders and around subtle perihilar opacities. Foundational results establish compactly supported biorthogonal bases with linear-phase symmetry and exact reconstruction [4]. We also evaluate Haar, Daubechies, Coiflet, and Symlet at level-1, and we compare Bior6.8 at level-1 with a deeper level-4 variant. The set of available discrete wavelet families.

3.4 Feature extraction

From each sub-band we compute a compact set of first-order statistics and GLCM-based texture descriptors, then concatenate across bands to form a tabular vector, as seen in Fig. 1.

1. First-order per sub-band: minimum, maximum, mean, standard deviation.

2. Texture per sub-band from gray-level co-occurrence matrices: energy, entropy, homogeneity, contrast, dissimilarity, correlation. We compute GLCMs at four orientations: $0, 45, 90, 135$ at unit distance and average properties over orientations. The definitions of these properties follow the scikit-image documentation, which implements the standard Haralick family.

This yields a 40–44-D vector in our implementation. The design captures global density in LL, and oriented texture in LH, HL, and HH, which radiologists use to judge air-space disease. The classical source for co-occurrence texture features is Haralick et al. and we follow those definitions.

3.5 Machine Learning algorithms

We use two tree-based learners suited to compact tabular features and amenable to feature attribution: Random Forest and XGBoost. These models avoid the heavy compute of large CNNs while remaining strong on multiscale texture features.

3.6 Ablations

We probe where performance comes from with three targeted ablations.

1. Sub-band contribution compares LL only, each detail band alone, pairwise combinations with LL, LL+LH+HL, and LL+LH+HL+HH. This tests scale and orientation complementarity.

2. Wavelet family and depth compares Bior6.8 with Haar, Daubechies, Coiflet, and Symlet at level-1, and contrasts Bior6.8 at level-1 versus level-4. This tests edge preservation and the bias–variance trade-off in multiresolution analysis.

3. Descriptor importance removes groups and single statistics to test the hypothesis that texture carries most of the discriminative signal on CXR.

4 Results

4.1 Comparison with DCNN baselines

Across the different pretrained backbones fine-tuned with Strategy I [2], test accuracies fall between 90 and 94 with pre-trained VGG16 at 94.38%. Strategy II shows a similar band with small model-dependent shifts, for example VGG16 at 95.20% and ResNet50 at 93.63%. Table 1 aggregates these DCNN results and places them next to our compact pipeline. Using a one-level Bior6.8 DWT with forty-four handcrafted statistics and textures coupled to XGBoost, the held-out test accuracy reaches 97.76%, exceeding the best DCNN values under either strategy despite a dramatically smaller feature space and no heavy preprocessing. The same feature stack with Random Forest attains 96.83%, again competitive with or above the DCNNs.

In supervised imaging a model is the full end-to-end pipeline that maps pixels to predictions. This includes deterministic preprocessing. Standard works formalize the pipeline as a single evaluable

Table 1: Comparison of transfer-learning DCNNs under two preprocessing strategies with the proposed wavelet–tabular pipeline on the same four-class CXR dataset. Accuracy and macro-averaged Precision, Recall, and F1 are reported. **Strategy I** applies CLAHE and a blackhat morphological operation. **Strategy II** uses raw images without preprocessing [2].

Method	Accuracy (%)	Macro P (%)	Macro R (%)	Macro F1 (%)
DenseNet201$_I$	90.99	90.60	90.30	90.40
DenseNet201$_{II}$	92.31	91.90	91.60	91.70
MobileNet$_I$	92.79	92.30	92.00	92.10
MobileNet$_{II}$	90.14	89.70	89.40	89.50
ResNet50$_I$	93.40	93.00	92.80	92.90
ResNet50$_{II}$	93.63	93.20	93.00	93.10
VGG16$_I$	94.38	94.60	94.40	94.50
VGG16$_{II}$	95.20	95.30	95.10	95.20
Xception$_I$	93.51	93.00	92.80	92.90
Xception$_{II}$	92.92	92.50	92.30	92.40
This work				
XGB + Bior6.8 (Level-1)	97.76	**97.5**	**97.5**	**97.5**
RF + Bior6.8 (Level-1)	96.83	96.50	96.50	96.50

object, and best-practice checklists in medical imaging require that preprocessing be specified as part of the method [20]. Under this view, comparing our wavelet–tabular system to transfer-learning DCNN pipelines that embed CLAHE and morphological enhancement is appropriate when task, labels, split, and metric are matched. Our previous work used the same four-class dataset family with transfer-learning DCNNs and reported Strategy I results in the 90.99–94.38% range across DenseNet201, ResNet50, Xception, MobileNet, and VGG16 [2]. On the same family, one-level Bior6.8 with forty-four handcrafted features and XGBoost achieves 97.76% test accuracy. Read together with our ablations, these findings support the claim that multiscale, orientation-aware textures are a stronger and more practical alternative to high-capacity transfer learning for four-class CXR on this dataset family [2].

A second part of the claim is efficiency and memory. CNN backbones carry tens to hundreds of megabytes of weights. VGG16, ResNet50, DenseNet201, Xception, and MobileNet contain 138.4, 25.6, 20.2, 22.9, and 4.3 million parameters respectively. In contrast, our feature extractor is a single-level wavelet transform with a 44-dimensional output, and the downstream learner is a tree ensemble whose footprint scales with the number and depth of trees rather than with convolutional channels. XGBoost is designed for memory-efficient training and CPU-speed inference. On a 44-dimensional representation, training and inference run on CPU with a model size that is suitable for embedded or clinical desktop deployment.

4.2 A compact wavelet–tabular pipeline is competitive on multi-class CXR

Table 2: Per-class metrics for XGBoost with Bior6.8 (level-1) on the held-out test set. Macro and weighted averages summarize overall performance.

Class	Precision	Recall	F1
Healthy	0.98	0.98	0.98
COVID-19	0.97	0.98	0.97
Bacterial Pneumonia	0.97	0.96	0.96
Viral Pneumonia	0.98	0.98	0.98
Macro Avg.	0.98	0.98	0.98
Weighted Avg.	0.98	0.98	0.98

Using all four DWT sub-bands and the full 44-feature vector, our models reach 96.83% accuracy with Random Forest and 97.76% with XGBoost on the held-out set. Removing wavelet features drops performance to 88.5% and 89.3%, showing that multiscale structure is the main driver rather
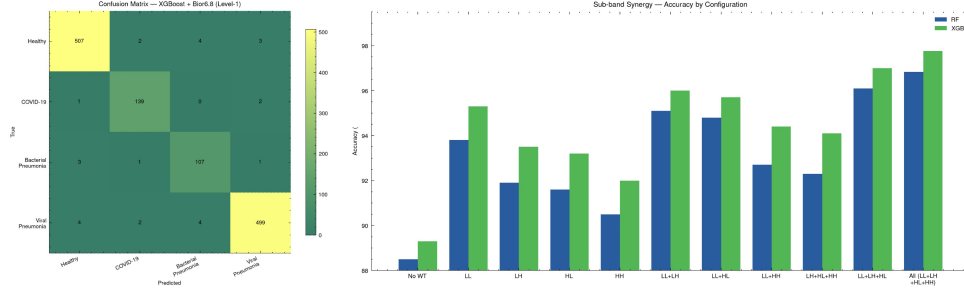
Figure 2: Caption

than raw intensities. This aligns with prior evidence that texture-centric representations capture radiographically meaningful variation in CXRs and can rival heavier CNNs when datasets are modest and labels are heterogeneous. A previous study on CXR pneumonia showed strong performance from textural biomarkers such as radiomics and related descriptors with classical learners, reinforcing that compact texture features are effective and easy to implement [17]. Table 2 details these per-class metrics and macro as well as weighted averages, and Fig. 1a visualizes the confusion matrix for XGBoost with Bior6.8 at level-1. The matrix is sharply diagonal with only a handful of false positives between Healthy and the two pneumonia classes, and minimal confusion between COVID-19 and Bacterial Pneumonia, which are often challenging to separate on frontal radiographs. Haralick features summarize how gray levels co-occur in a neighborhood. They are computed from a gray-level co-occurrence matrix and capture contrast, homogeneity, energy, entropy, and correlation, which track heterogeneity and edges that radiologists associate with opacities [6, 3]. Local binary patterns threshold each pixel's neighborhood against the center to form a binary code that is robust to monotonic gray-scale changes and sensitive to micro-patterns such as edges and spots [16].

4.3 Sub-band synergy and texture importance

Fig. 1b aggregates headline accuracies for different sub-band selections.

The feature ablation heatmap in Fig. 2 shows that texture is the primary carrier of discriminative information. Removing the texture group—energy, entropy, homogeneity, contrast, dissimilarity, correlation—produces the largest drop, 6.0% for RF and 3.7% for XGB. Excluding any single first-order statistic causes only small changes, typically less than 0.3% for RF. This matches the radiologic view that texture encodes heterogeneity in aeration and consolidation. It also aligns with classical GLCM theory, where co-occurrence statistics summarize local gray-level relationships that track edges, clumping, and mottled opacities [22, 6].

Independent studies support this emphasis on texture for CXRs. Ortiz-Toro and colleagues showed that textural biomarkers, including radiomics, can detect pneumonia effectively across public datasets using classical learners [17]. Kim demonstrated that a small set of GLCM features can separate COVID-19 from non-COVID pneumonia on a bias-minimized single-institution cohort, with the most influential variables drawn from contrast and difference-variance [11]. LBP-based pipelines also report strong performance when paired with SVM or related classifiers, indicating that micro-pattern codes carry diagnostically useful information in chest radiographs [15]. Broader texture-centric frameworks that fuse LBP, HOG, and Haralick families further corroborate the value of handcrafted texture on CXR tasks under limited data [7]. Taken together, our ablations show that multiscale information works best when sub-bands are combined. The evidence from radiomics and LBP studies explains why. Texture features capture distribution and clustering of opacities that define pneumonia on radiographs. First-order intensity alone carries signal, yet it is the multiresolution texture that consistently closes the gap to state-of-the-art performance.

4.4 Wavelet family and depth

At level-1, Bior6.8 is the top performer, reaching highest accuracy above 6-8 % points over Haar, Daubechies, Coiflet, and Symlet cluster which achieve near 90–92%. This confirms that the choice of mother wavelet drives accuracy in our setting. Bior6.8's linear-phase and near-symmetric anal-
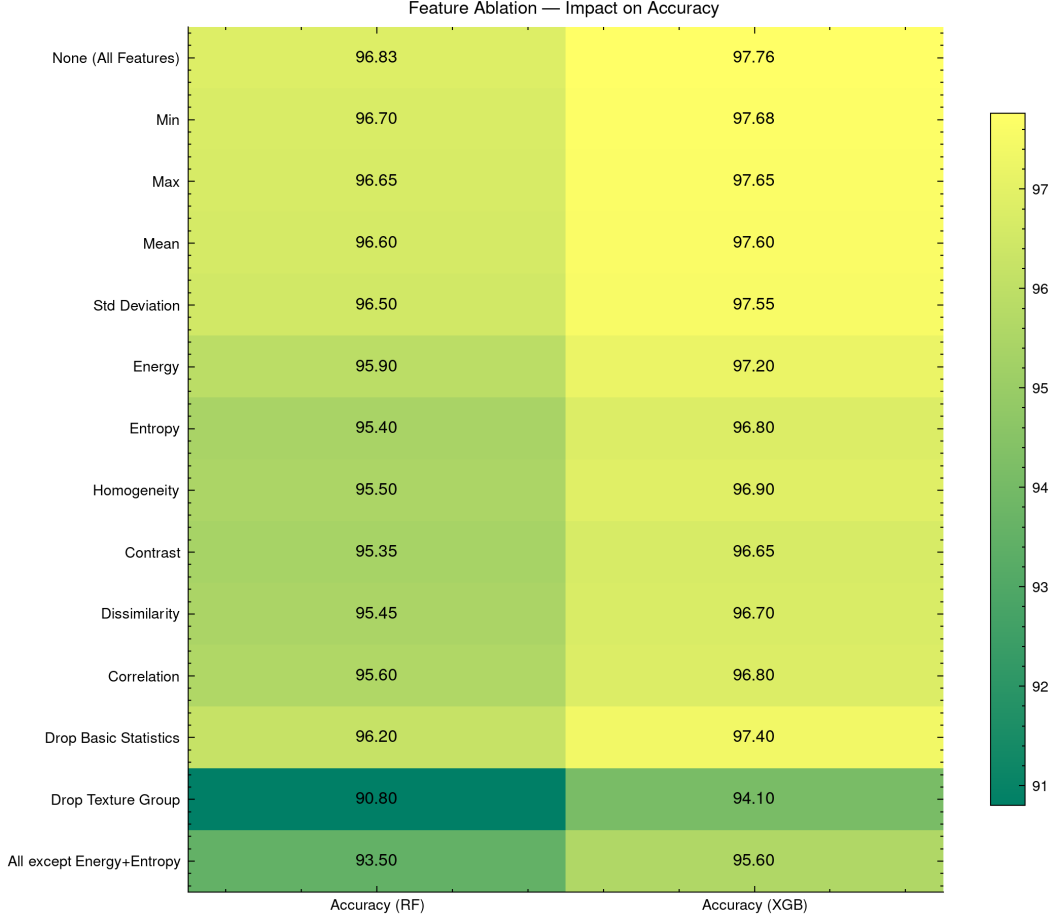
Figure 3: Caption

ysis–synthesis filters preserve edges and reduce phase distortion, which is desirable around lung borders and subtle perihilar opacities. Authoritative references describe linear-phase realizations for biorthogonal families and explain why edge structure is better maintained than with many orthogonal designs [21]. With limited data, deeper decompositions can inject redundant fine-scale coefficients and expand the feature space without adding stable signal. In our experiments, Bior6.8 at four levels performs worse (93.3% RF, 93.2% XGB) than single-level Bior6.8 (96.8%, 97.8%). The single-level setting captures coarse and mid-scale texture with fewer features and better generalization. This pattern is consistent with standard bias–variance considerations for small datasets. Directional multiscale context. For a compact and auditable feature space, level-1 Bior6.8 offers a sound default. It aligns with theory on biorthogonal, linear-phase filter banks and it matches what we observe empirically on multi-class CXR classification.

5 Conclusion

We introduced a lightweight multiclass CXR pipeline that uses a single level wavelet transform and compact texture descriptors to classify healthy cases, COVID-19, bacterial pneumonia, and viral pneumonia, and we showed that tabular learners outperform transfer-learned DCNN baselines on the same data. The main limitation is scope: our labels cover a narrow set of thoracic findings, so the next step is to include more clinically relevant CXR categories and to benchmark alongside complementary CT workflows that often serve as the reference standard for pneumonia assessment. Directional multiscale representations such as shearlets are a natural extension for the future work. Shearlets encode anisotropic, edge-like structures with high directional selectivity and sparse approximation, which matches pulmonary anatomy better than isotropic wavelets. Building on these

findings, our next step is to integrate shearlet based descriptors into the same lightweight pipeline, which have been reported to surpass wavelet features, as well as outperform end-to-end deep baselines on small, heterogeneous datasets.

References

[1] Lamiaa Abdel-Hamid. Multiresolution analysis for covid-19 diagnosis from chest ct images: wavelet vs. contourlet transforms. *Multimedia Tools and Applications*, 83(1):2749–2771, 2024.

[2] Amitesh Badkul, Inturi Vamsi, and Radhika Sudha. Comparative study of dcnn and image processing based classification of chest x-rays for identification of covid-19 patients using fine-tuning. *Journal of Medical Engineering & Technology*, 48(6):213–222, 2024.

[3] Patrik Brynolfsson, David Nilsson, Turid Torheim, Thomas Asklund, Camilla Thellenberg Karlsson, Johan Trygg, Tufve Nyholm, and Anders Garpebring. Haralick texture features from apparent diffusion coefficient (adc) mri images depend on imaging and pre-processing parameters. *Scientific reports*, 7(1):4041, 2017.

[4] Albert Cohen, Ingrid Daubechies, and J-C Feauveau. Biorthogonal bases of compactly supported wavelets. *Communications on pure and applied mathematics*, 45(5):485–560, 1992.

[5] Rishi Gadepally, Andrew Gomella, Eric Gingold, and Paras Lakhani. Generalization of artificial intelligence models in medical imaging: A case-based review. *arXiv preprint arXiv:2211.13230*, 2022.

[6] Robert M Haralick, Karthikeyan Shanmugam, and Its' Hak Dinstein. Textural features for image classification. *IEEE Transactions on systems, man, and cybernetics*, (6):610–621, 2007.

[7] Jamal N Hasoon, Ali Hussein Fadel, Rasha Subhi Hameed, Salama A Mostafa, Bashar Ahmed Khalaf, Mazin Abed Mohammed, and Jan Nedoma. Covid-19 anomaly detection and classification method based on supervised machine learning of chest x-ray images. *Results in Physics*, 31:105045, 2021.

[8] Giovanni Irmici, Maurizio Cè, Elena Caloro, Natallia Khenkina, Gianmarco Della Pepa, Velio Ascenti, Carlo Martinenghi, Sergio Papa, Giancarlo Oliva, and Michaela Cellina. Chest x-ray in emergency radiology: What artificial intelligence applications are available? *Diagnostics*, 13(2):216, 2023.

[9] S Kavitha and Hannah Inbarani. Bayes wavelet-cnn for classifying covid-19 in chest x-ray images. In *Computational Vision and Bio-Inspired Computing: ICCVBIC 2020*, pages 707–717. Springer, 2021.

[10] Ejaz Khan, Muhammad Zia Ur Rehman, Fawad Ahmed, Faisal Abdulaziz Alfouzan, Nouf M Alzahrani, and Jawad Ahmad. Chest x-ray classification for the detection of covid-19 using deep learning techniques. *Sensors*, 22(3):1211, 2022.

[11] Young Jae Kim. Machine learning model based on radiomic features for differentiation between covid-19 and pneumonia on chest x-ray. *Sensors*, 22(17):6709, 2022.

[12] Mengfang Li, Yuanyuan Jiang, Yanzhou Zhang, and Haisheng Zhu. Medical image analysis using deep learning algorithms. *Frontiers in public health*, 11:1273253, 2023.

[13] Stephane G Mallat. A theory for multiresolution signal decomposition: the wavelet representation. *IEEE transactions on pattern analysis and machine intelligence*, 11(7):674–693, 2002.

[14] Sayed Amir Mousavi Mobarakeh, Kamran Kazemi, Ardalan Aarabi, and Habibollah Danyal. Empowering medical imaging with artificial intelligence: A review of machine learning approaches for the detection, and segmentation of covid-19 using radiographic and tomographic images. *arXiv preprint arXiv:2401.07020*, 2024.

[15] Auwalu Saleh Mubarak, Sertan Serte, Fadi Al-Turjman, Zubaida Sa'id Ameen, and Mehmet Ozsoz. Local binary pattern and deep learning feature extraction fusion for covid-19 detection on computed tomography images. *Expert Systems*, 39(3):e12842, 2022.

[16] Timo Ojala, Matti Pietikainen, and Topi Maenpaa. Multiresolution gray-scale and rotation invariant texture classification with local binary patterns. *IEEE Transactions on pattern analysis and machine intelligence*, 24(7):971–987, 2002.

[17] César Ortiz-Toro, Angel García-Pedrero, Mario Lillo-Saavedra, and Consuelo Gonzalo-Martin. Automatic detection of pneumonia in chest x-ray images using textural features. *Computers in biology and medicine*, 145:105466, 2022.

[18] Andreas S Panayides, Amir Amini, Nenad D Filipovic, Ashish Sharma, Sotirios A Tsaftaris, Alistair Young, David Foran, Nhan Do, Spyretta Golemati, Tahsin Kurc, et al. Ai in medical imaging informatics: current challenges and future directions. *IEEE journal of biomedical and health informatics*, 24(7):1837–1857, 2020.

[19] Luís Pinto-Coelho. How artificial intelligence is shaping medical imaging technology: a survey of innovations and applications. *Bioengineering*, 10(12):1435, 2023.

[20] Umaseh Sivanesan, Kay Wu, Matthew DF McInnes, Kiret Dhindsa, Fateme Salehi, and Christian B van der Pol. Checklist for artificial intelligence in medical imaging reporting adherence in peer-reviewed and preprint manuscripts with the highest altmetric attention scores: a meta-research study. *Canadian Association of Radiologists Journal*, 74(2):334–342, 2023.

[21] Hwee Huat Tan, Li-Xin Shen, and Jo Yew Tham. New biorthogonal multiwavelets for image compression. *Signal Processing*, 79(1):45–65, 1999.

[22] Bino A Varghese, Steven Y Cen, Darryl H Hwang, and Vinay A Duddalwar. Texture analysis of imaging: what radiologists need to know. *American Journal of Roentgenology*, 212(3):520–528, 2019.

[23] Jingyu Xu, Binbin Wu, Jiaxin Huang, Yulu Gong, Yifan Zhang, and Bo Liu. Practical applications of advanced cloud services and generative ai systems in medical image analysis. *arXiv preprint arXiv:2403.17549*, 2024.

[24] Huseyin Yasar and Murat Ceylan. A new deep learning pipeline to detect covid-19 on chest x-ray images using local binary pattern, dual tree complex wavelet transform and convolutional neural networks. *Applied Intelligence*, 51(5):2740–2763, 2021.